

# A Model-Based Approach for Detection of Objects in Low Resolution Passive-Millimeter Wave Images\*

Yuan-Liang Tang, Sadashiva Devadiga, and Rangachar Kasturi\*\*  
The Pennsylvania State University

and

Randall L. Harris, Sr.  
NASA Langley Research Center

77-54  
10-147  
10-10

## Abstract

We describe a model-based vision system to assist the pilots in landing maneuvers under restricted visibility conditions. The system has been designed to analyze image sequences obtained from a Passive Millimeter Wave (PMMW) imaging system mounted on the aircraft to delineate runways/taxiways, buildings, and other objects on or near runways. PMMW sensors have good response in a foggy atmosphere; but their spatial resolution is very low. However, additional data such as airport model and approximate position and orientation of aircraft are available. We exploit these data to guide our model-based system to locate objects in the low resolution image and generate warning signals to alert the pilots. We also derive analytical expressions for the accuracy of the camera position estimate obtained by detecting the position of known objects in the image.

## I. Introduction

Federal regulations specify the minimum visibility conditions under which airlines may take off and land. These minima are a function of the types of airplane and airport equipment. Therefore, there is a great deal of interest in imaging sensors which can *see through* fog and produce a *real world* display which, when combined with symbolic or pictorial guidance information, could provide the basis for a landing system with lower visual minimum capability than those presently being used [1].

Since the energy attenuation in the visible spectrum due to fog is very large [2] (Fig.1), sensors are being designed to operate at lower frequencies (e.g. 94 GHz) where the attenuation is lower providing the ability to see through fog. NASA Langley Research Center, in cooperation with industry, is performing research on an on-board imaging system using a passive sensor operating at this frequency. Images from such sensors are of very low spatial resolution (Fig. 2). However, additional supporting information in the form of knowledge about the airport and the position, orientation and velocity of aircraft is generally available. Thus a model-based image analysis approach is feasible to segment the image and to detect and track objects on the ground. Information

\* This research is supported by a grant from NASA Langley Research Center, Hampton, Virginia (NAG-1-1371).

\*\* Address all correspondence to Professor Rangachar Kasturi (kasturi@cmpe.psu.edu).

extracted from such an analysis is useful to generate warning signals to the pilot of any potential hazards. This paper describes such a model-based technique, which makes use of a priori information about the geometric model of the airport and camera position and attitude data provided by the Global Positioning System (GPS) and other instruments.

The geometric model of the airport contains positions of the runways/taxiways and buildings, the navigation instruments provide the position of the aircraft, and on-board instruments provide the orientation of the aircraft (yaw, pitch and roll). We use this information to define regions of interest in the image where important features such as runways/taxiways, the horizon, etc. are likely to be present. Edges corresponding to these features of interest are detected within these regions. After delineating regions representing runway/taxiways, we look for objects inside and outside these regions.

The data from radio navigation instruments are known only upto a certain accuracy depending upon the type of radio navigation instruments. For example, GPS data is updated once every second and it is likely that a few such updates are missed making camera position data to be a few hundred feet off. On-board instrument data is generally useful to obtain more accurate camera position data than the GPS-based data. An alternative approach is to use the information about the location of detected objects in the images with known world coordinates (e.g. intersection of runways/taxiways, corners of buildings, etc.) to obtain an improved estimate of the camera position. This requires an analytical study of the relationships among the camera parameters, the resolution of the images, and the distances between the aircraft and objects.

In Section II we present a block diagram of the complete system. In Section III we describe the analytical model that establishes the relationship between the position, orientation and other physical parameters of the camera and the attributes of the captured images. This model is useful to calculate the accuracy of camera position estimation using image based features. In Section IV we present the method for defining the regions of interest in the image using the camera parameters and airport model. Section V includes image processing steps that are used to find regions corresponding to major features in the image and to detect objects in these regions. Experimental results are presented in Section VI. We conclude the paper with a summary and a brief description of future work.

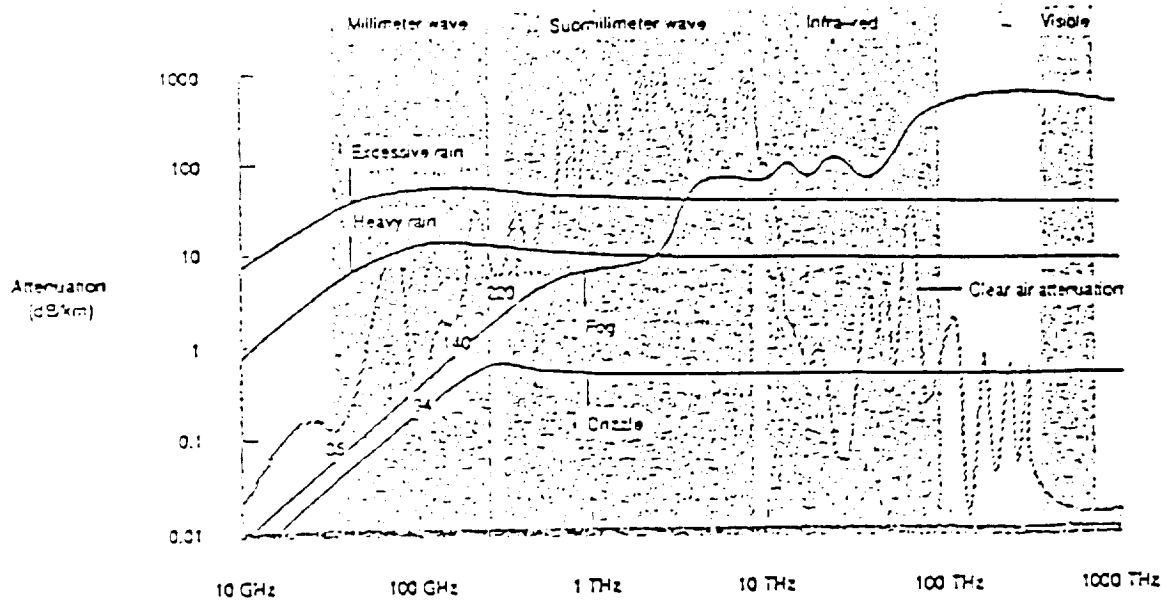


Fig. 1. Atmospheric effects on electromagnetic radiation [2].



Fig. 2. The Passive Millimeter Wave image.

## II. System Description

In this section, we describe the functions of various modules of the system shown in Fig.3 and the interactions between them. The input model of the airport contains positions of the runways/taxiways, and buildings. The *model transformation* module will take this model and the camera state information (position and orientation) as inputs to define the regions of interest in the image plane.

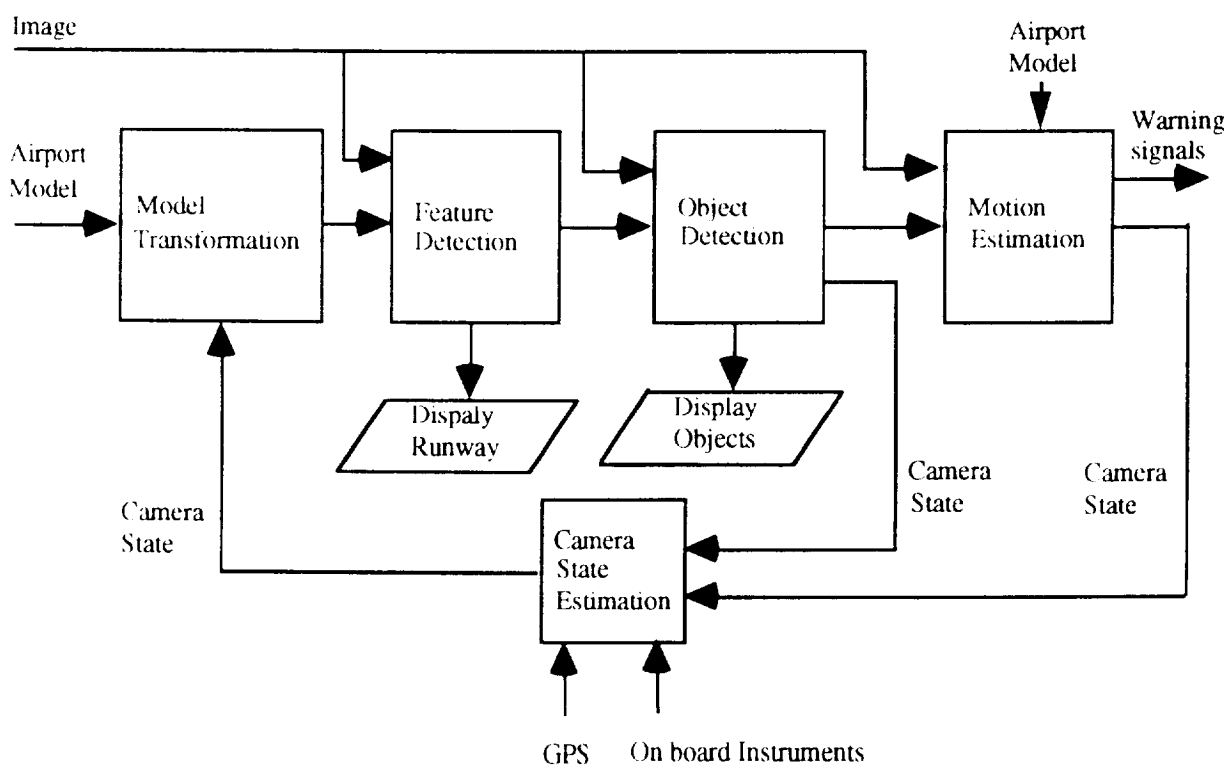


Fig. 3. System block diagram.

The image processing algorithms in the *feature detection* module operates within these regions of interest to detect the edges of the runway, horizon, etc. in the image. An edge is fitted to the edge pixels if enough edge pixels are found within the region of interest. The module outputs parameters which define major regions in the input image.

The *object detection* module detects objects in the image using different thresholds for each region. For example, since detection of objects on the runway is extremely important, a lower threshold is used to flag every object even if the contrast is low whereas a higher threshold is used to detect objects which are outside the runway such as buildings, etc. Locations of detected objects with known world coordinates is useful to estimate camera state parameters.

The *motion estimation module* uses dynamic scene analysis methods to estimate camera state parameters as well as to detect velocities of objects on the ground. The outputs from this module will be useful to detect potential collisions and generate warning signals as appropriate.

The *camera state estimation* module integrates information obtained about the position and velocity of the aircraft from various sensors and modules and outputs necessary data to the *model transformation* module.

### III. Accuracy of Camera State Estimation from Image-based Features

As we need to use the camera state estimated from locating features of known objects in the image during the period when the GPS is not updated, it is necessary to know the accuracy of such estimated positions and the factors that decide the accuracy. Hence, an analytical model that establishes the relationship between the camera parameters and the attributes of captured images is necessary for guiding the image analysis system. Sensor positional parameters include range (distance from the aircraft to the runway threshold), cross range (distance from the aircraft to the runway center line), altitude, and pitch, roll and yaw angles. Sensor imaging attributes include the number of pixels in the image and the optical angular view measured in degrees. We derive the inter-relationships among these parameters. Using these relationships we calculate the accuracy of the estimate of camera position based on a minimum resolvable movement of features by one pixel in the image. We obtain these accuracies for three different types of cameras (PMMW, FLIR, HDTV) at six ranges.

#### A. Analysis

Throughout the analysis, for convenience, we assume that the sensor is located at the center of gravity of the airplane. Hence we can use the terms sensor position and aircraft position interchangeably. We also neglect the effect of curvature of the earth. The system of reference axis that forms the basis of system of notations used to describe the position of the sensor is shown in Fig. 4. The figure shows an airplane with three mutually perpendicular axes — pitch, roll and yaw — passing through the center of gravity of the airplane. The three angular displacements are termed pitch, roll and yaw as shown in Fig. 4. The image plane is assumed to be perpendicular to the rolling axis with its vertical and horizontal axes coinciding with the yawing and the pitching axis of the airplane, respectively.

Fig. 5 shows an imaging situation during landing where the aircraft is at  $(X_c, Y_c, Z_c)$ , with pitching angle  $\theta$ , zero yaw and zero roll angle. Let  $\alpha = 90 - \theta$ . The field of view of the camera is determined by two viewing angles:  $\Delta\alpha$  defined in the same plane as  $\theta$  and  $\Delta\beta$  at right angles to  $\Delta\alpha$  ( $\Delta\alpha$  determines the vertical extent of the image and  $\Delta\beta$  its horizontal extent). Even though the image obtained by the sensor is always a rectangle, the ground area captured by the sensor is a trapezoid  $ABCD$  whose side length and area depends on  $\Delta\alpha$ ,  $\Delta\beta$  and various other sensor

parameters like position, orientation etc. Note that a pixel in the image plane corresponds to a patch on the ground plane. We refer to this as a pixel-patch (see Fig. 6).

Consider a point feature which has been detected at some pixel  $(p, q)$ . Let the actual world coordinates of this feature be  $(P, Q, 0)$ . Since a pixel represents a patch on the ground, the camera could change in its position by certain amount while still retaining the image of the feature at the same pixel  $(p, q)$ . Hence a camera pose estimation by passive triangulation will always give the same camera pose for nearby camera positions unless the change in camera position is large enough for the feature to be observed in the neighboring pixel. We define this minimum change in camera displacement as the sensitivity of the camera. Note that this is a measure of accuracy of camera position estimate and is a function of the camera, image size in number of pixels, angular resolution, and the pixel location  $(p, q)$  in the image plane.

Let  $N_x$  and  $N_y$  represent the number of pixels in the vertical and horizontal directions, respectively. The pixels are numbered  $-N_x/2, \dots, 0, \dots, N_x/2-1$  in the vertical direction and  $-N_y/2, \dots, 0, \dots, N_y/2-1$  in the horizontal direction. The rolling axis of the plane is assumed to pass through the bottom right corner of the patch on the ground plane which corresponds to the center pixel in the image plane. Other pixels are referenced in a similar manner. The coordinates of the reference corner of the ground area covered by a pixel  $(p, q)$  can be estimated by the following relations.

$$\begin{aligned} X &= X_c + Z_c \tan\left(\alpha + p \frac{\Delta\alpha}{N_x}\right) \\ Y &= Y_c + \frac{Z_c}{\cos\left(\alpha + p \frac{\Delta\alpha}{N_x}\right)} \tan\left(q \frac{\Delta\beta}{N_y}\right) \end{aligned} \quad (1)$$

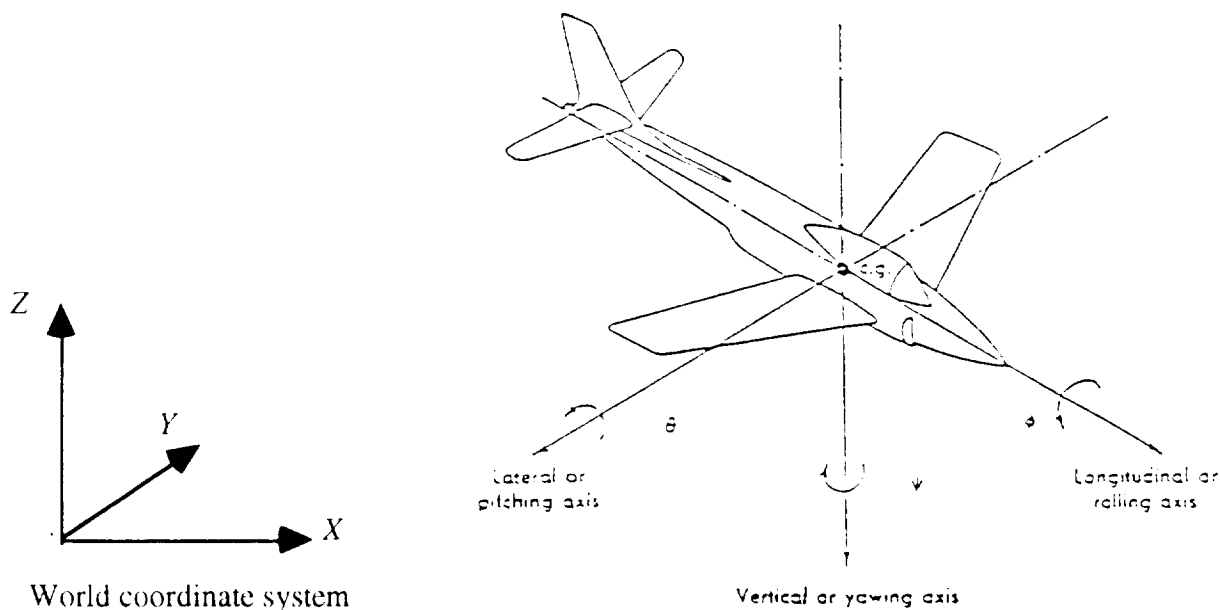


Fig. 4. Airplane-body axis (Reproduced from "Airplane Aerodynamics" by Dommasch and Danieol Otto [ed. 1967]).

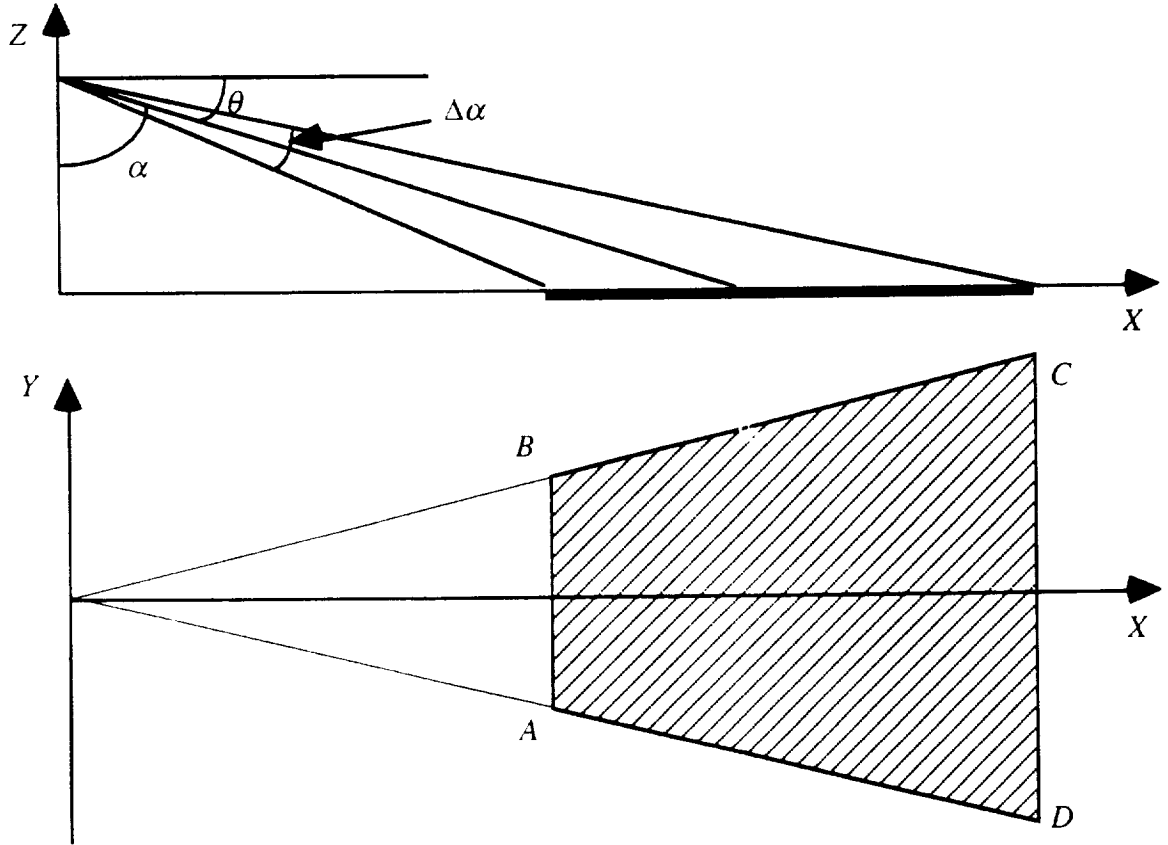


Fig. 5. Image obtained by the sensor is projected towards the ground. Hatched portion is the ground area covered by the sensor.

For a non zero rolling angle  $\phi$ , the ground coordinates  $(X', Y')$  which corresponds to a pixel  $(p, q)$  in the image plane are obtained by replacing  $(p, q)$  in the above equation by  $(p', q')$ , where

$$\begin{aligned} p' &= p \cos \phi - q \sin \phi, \\ q' &= p \sin \phi + q \cos \phi. \end{aligned} \quad (2)$$

Since a pixel-patch is referenced by its bottom right corner of the pixel, the other three corners become the reference of its three neighboring pixels-patch as shown in Fig. 7. Thus, the four corners of this pixel-patch,  $(X_i', Y_i')$ ,  $i=1,2,3,4$ , are obtained by using Eq. (1), where  $(p, q)$  are replaced by  $(p_i', q_i')$ , where

$$\begin{aligned} p_i &= p_i \cos \phi - q_i \sin \phi, \\ q_i &= p_i \sin \phi + q_i \cos \phi. \end{aligned} \quad (3)$$

and  $(p_1, q_1) = (p, q)$ ,  $(p_2, q_2) = (p+1, q)$ ,  $(p_3, q_3) = (p+1, q+1)$ , and  $(p_4, q_4) = (p, q+1)$ .

Eq. (1) explicitly gives the relationship between the camera parameters  $(X_c, Y_c, Z_c)$ ,  $\theta$ ,  $\phi$ , and a ground point corresponding to a pixel  $(p, q)$ . We are now interested in computing the sensitivity of the imagery sensor. This is defined as the minimum change in a camera parameter that

would move a fixed ground point to the next pixel in the image plane. We obtain this by taking the partial derivative of  $X_1'$  and  $Y_1'$  with respect to the corresponding parameter. For example,

$$D_{X_c}^X = \frac{\partial X_1'}{\partial X_c}, \text{ and } D_{X_c}^Y = \frac{\partial Y_1'}{\partial X_c}. \quad (4)$$

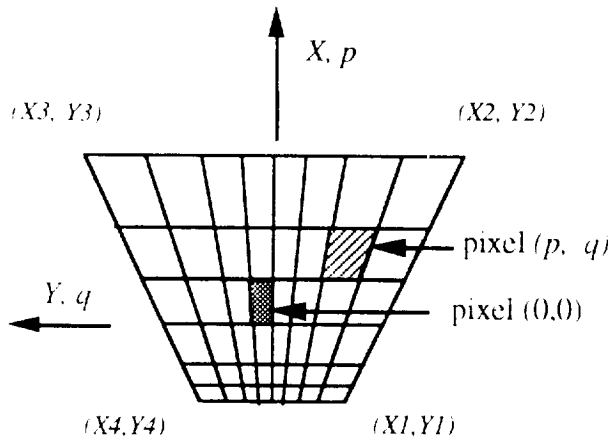


Fig. 6. Ground area covered by the sensors. Each small trapezoid corresponds to a pixel in the actual image.

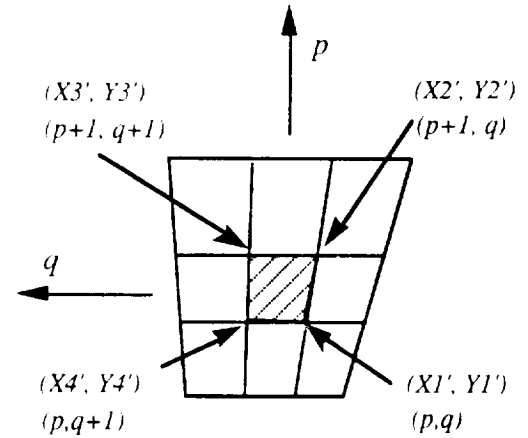


Fig. 7. A pixel  $(p, q)$  projected towards the ground.

This derivation is an approximation to the amount of change in  $X_1'$  for unit change in  $X_c$ . Thus we estimate that the amount of change in  $X_c$  in order to change  $X_1'$  to  $X_2'$ , or  $Y_1'$  to  $Y_4'$  (which define the corners of adjacent pixels) as

$$S_{X_c} = \frac{(X_2' - X_1')}{D_{X_c}^X}, \text{ and } S_{X_c}^Y = \frac{(Y_4' - Y_1')}{D_{X_c}^Y}. \quad (5)$$

Note that  $S_{X_c}^Y = \infty$ , as expected. Sensitivity with reference to other parameter is defined in a similar manner. These are summarized in Table I.

Sensor sensitivity is a function of various sensor parameters and sensor attitudes. Since the sensor plane is inclined to the ground plane, the sensitivity varies in the vertical and horizontal direction along the sensor plane and hence is a function of pixel number  $(p, q)$ . Equivalently, the accuracy of estimation of sensor position using ground truth data is a function of pixel position as well as other parameters. For a given range, the estimation using features that are observed at the top half of the sensor are less accurate because of the large ground area represented by these pixels. Also for a given  $p$ , the accuracy decreases as we move towards the border of the sensor in the horizontal direction. In summary, the accuracy of estimation is a function of sensor characteristic and the ratio of the sensor view angle to the number of pixels in the image.

SPP		Sensor Sensitivity at (p, q)	Sensor Sensitivity at (0, 0) with $\phi = 0$
$X_c$	$S_x^x$	$2 Z_c \sin(\cos\phi \cdot \Delta\alpha/N_x) / \{\cos[2\alpha + \Delta\alpha/N_x \{ (2p+1)\cos\phi - 2q\sin\phi \}] + 1\}$	$2 Z_c \sin(\Delta\alpha/N_x) / \{\cos[2\alpha + \Delta\alpha/N_x] + 1\}$
	$S_x^y$	$\infty$	$\infty$
$Y_c$	$S_y^x$	$\infty$	$\infty$
	$S_y^y$	$\{Z_c \tan(q_4' \Delta\beta / N_y) / \cos(\alpha + p_4' \Delta\alpha / N_x)\} - \{Z_c \tan(q_1' \Delta\beta / N_y) / \cos(\alpha + p_1' \Delta\alpha / N_x)\}$	$2 Z_c \sin(\Delta\beta/N_y) / \{\cos\alpha \cdot \cos(\Delta\beta/N_y) + 1\}$
$Z_c$	$S_z^x$	$S_x^x / \tan(\alpha + p_1' \Delta\alpha / N_x)$	$2 Z_c \sin(\Delta\alpha/N_x) / \sin(2\alpha + \Delta\alpha/N_x)$
	$S_z^y$	$S_y^y \cos(\alpha + p_1' \Delta\alpha / N_x) / \tan(q_1' \Delta\beta / N_y)$	$\infty$
$\theta$	$S_\theta^x$	$S_x^x \cos^2(\alpha + p_1' \Delta\alpha / N_x) / Z_c$	$\sin(\Delta\alpha/N_x) / \{\cos\alpha / \cos(\alpha + \Delta\alpha/N_x)\}$
	$S_\theta^y$	$S_y^y \cos^2(\alpha + p_1' \Delta\alpha / N_x) / Z_c \tan(q_1' \Delta\beta / N_y) \sin(\alpha + p_1' \Delta\alpha / N_x)$	$\infty$
$\phi$	$S_\phi^x$	$S_x^x \cos^2(\alpha + p_1' \Delta\alpha / N_x) / (Z_c \Delta\alpha / N_x) (-p \sin\phi - q \cos\phi)$	$\infty$
	$S_\phi^y$	$S_y^y / Z_c [A \delta B / \delta\phi + B \delta A / \delta\phi]$	$\infty$

$A = 1/\cos(\alpha + p_1' \Delta\alpha / N_x)$ ;  $B = \tan(q_1' \Delta\beta / N_y)$ ;  $\delta B / \delta\phi = (p \cos\phi - q \sin\phi) (\Delta\beta / N_y) \cos^2(q_1' \Delta\beta / N_y)$   
 $\delta A / \delta\phi = \tan(\alpha + p_1' \Delta\alpha / N_x) (-p \sin\phi - q \cos\phi) (\Delta\alpha / N_x) \cos(\alpha + p_1' \Delta\alpha / N_x)$ ;  $\alpha = 90 + \theta$ ;  
 $(p_1, q_1) = (p, q)$ ;  $(p_4, q_4) = (p, q+1)$ ;  $p_1' = p_1 \cos\phi - q_1 \sin\phi$ ;  $p_4' = p_4 \cos\phi - q_4 \sin\phi$ ;  
 $q_1' = p_1 \sin\phi + q_1 \cos\phi$ ;  $q_4' = p_4 \sin\phi + q_4 \cos\phi$

SPP: Sensor Positional Parameters		Sensor Characteristics	
$(X_c, Y_c, Z_c)$	Sensor position	Vertical	Horizontal
$\theta$	Pitch angle	$\Delta\alpha$	$\Delta\beta$
$\phi$	Roll angle	$N_x$	$N_y$

**Sensitivity:** Minimum change in the sensor positional parameters ( $X_c, Y_c, Z_c, \theta, \phi$ ) that will make the object to appear in the next pixel either in the vertical (X; hence called as sensitivity in x direction) or in the horizontal (Y; hence called as sensitivity in y direction) direction of the sensor plane.  $S_i^j$ : Sensitivity in the direction 'j' due to the sensor positional parameter 'i' computed at pixel (p, q) in the image plane.

Table I. Sensor positional sensitivity equations.

## B. Quantitative Results and Discussions

The sensitivity analysis described in the previous section was applied to three different sensors at six different positions (Table II). Sensitivities  $S_{X_c}^X$ ,  $S_{Y_c}^Y$  and  $S_{Z_c}^X$ , at the aim point (i.e.,  $p=0$ ,  $q=0$ ) for various sensor positions are plotted in Figs. 8, 9 and 10 respectively. Note that  $S_{Z_c}^Y$  is larger than  $S_{Z_c}^X$  at  $(0, 0)$  and hence a feature would move to the next horizontal pixel before it moves to the next vertical pixel. Thus only  $S_{Z_c}^X$  is important.

As expected, the sensitivity is the best for the sensor with the highest pixel resolution. Sensitivity also improves as the sensor is moved closer to the ground. It becomes poor for the features that are located at the far end of the vertical axis (top of the sensor), i.e., for the objects that are located at the far end of the runway. Thus, as expected, the position and velocity of the aircraft can be computed to a better accuracy by knowing the position of stationary objects on the ground that are closer to the aircraft.

The results indicate that the accuracy of camera state estimation would be no better than the GPS data unless a high resolution sensor is employed. Note that these results do not consider potential improvements that can be obtained by motion stereo techniques using a large number of image frames. We are presently investigating the possibility of improving the accuracy of the computed sensor positional parameters by extending our analysis using this method.

### Sensor Characteristic

<i>Sensor type</i>	<i>Pixel (H x V)</i>	<i>Field of View (H x V) deg.</i>
HDTV	1920 x 1035	30 x 24
FLIR	512 x 512	28 x 21
MMW	80 x 64	27 x 22

### Sensor Positions

<i>Location</i>	<i>Range in ft.</i>	<i>Altitude in ft.</i>
Threshold	0.0	50.0
CAT II - DH	908.1	100.0
CAT I -DH	2816.2	200.0
Middle Marker	4500.0	288.2
1000' Altitude	18081.1	1000.0
Outer Marker	29040.0	1574.3

In all the above six cases  
 Pitch angle -3.0 degree  
 Roll angle 0.0 degree  
 Cross Range 0.0 ft.

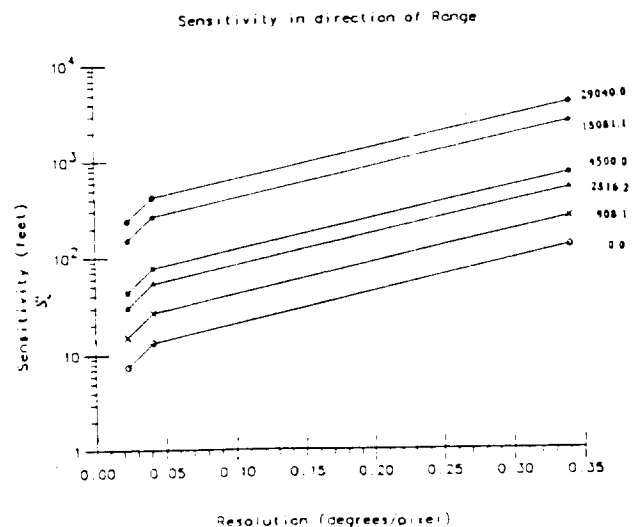


Table II.

Fig. 8.

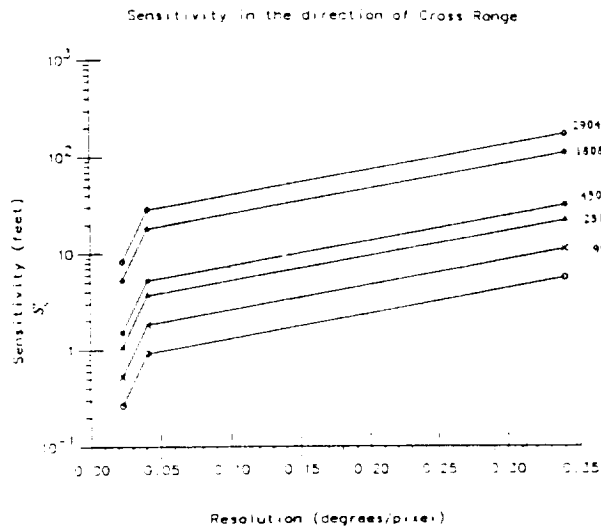


Fig. 9.

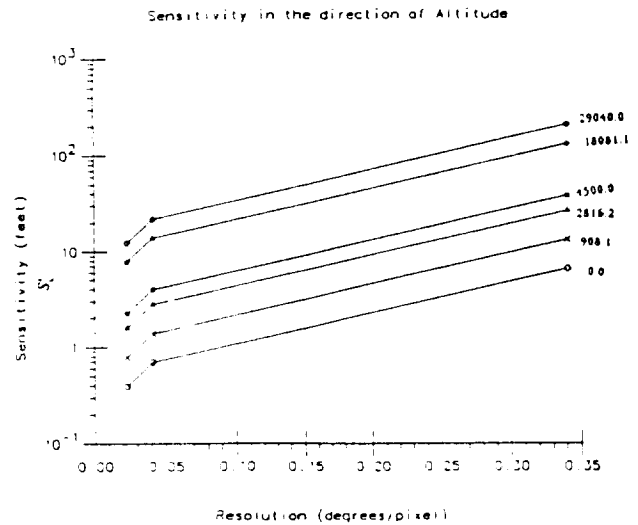


Fig. 10.

## IV. Model Transformation

As noted earlier, the PMMW images are low contrast-low resolution images. Simple edge detection techniques on these images generate many noisy edge pixels in addition to those belonging to the true edges such as runways, sky etc. This problem is alleviated by defining regions where the true edges are expected to occur using knowledge about the aircraft position and a model of the airport. The main functions of the *model transformation* module is to define a region of interest on the ground plane for each feature in the model and to perform 3D to 2D transformation. It also defines a region in the image plane where the horizon line should occur.

### A. Defining Regions of Interest for Runway Edges

The error in the expected location of a feature and its actual position in the image depends on several factors, most notably the accuracy of the camera position parameters used by the model transformation module. Furthermore, it is evident from our earlier analysis (Fig.6) that the ground area covered by a pixel is a function of the position of the pixel in the image. Thus it is not reasonable to define the search space for each feature as a fixed number of pixels centered around the expected location in the image plane. Hence we define the region of interest in the 3D space and then apply transformation to get the corresponding region of interest in the image. The extent of the search space in the 3D space is determined by the estimated error in camera positional parameters (which are based on GPS and on-board instrument data).

The geometric model of the airport contains a sequence of 3D coordinates of the vertices of the runway/taxiways, which forms a polygon with  $n$  vertices:

$$runway = \{P_i\}, i=1, 2, \dots, n.$$

where  $P_i = (X_i, Y_i, Z_i)^T$  is one of the vertices of the polygon. Note that  $Z_i = 0$ .  $P_i P_{i+1}$  specifies an edge of the polygon. The region of interest is defined as a rectangle on the ground which encloses the edge. Therefore, each edge  $P_i P_{i+1}$  of the polygon is associated with the region of interest

defined by four points  $b_j = (X_j, Y_j, Z_j)^T, j=1, \dots, 4$ , and  $Z_j = 0$ .

The width of the region of interest is defined as a function of the width of the runway/taxiway,  $w$ , accuracy of the GPS data,  $g$  ( $g \leq 1$ ), and the accuracy of the on-board instruments,  $d$  ( $d \leq 1$ ). Note that  $g$  and  $d$  are determined by the specification and characteristics of these instruments. This relationship is given by

$$\text{width}(w, g, d) = \frac{0.2w}{gd}. \quad (6)$$

Note that the minimum width is  $0.2w$  when  $g=d=1$ , which corresponds to  $\pm 10\%$  potential displacement of runway edge feature. To limit the search area from being a large fraction of the runway width we limit the search width to  $0.4w$  even if  $gd < 0.5$ .

After defining the region of interest for each edge, 3D to 2D coordinate transformation is performed using the following homogeneous equation [3]:

$$\begin{bmatrix} \lambda p \\ \lambda q \\ \lambda r \\ \lambda \end{bmatrix} = [P][R][T] \begin{bmatrix} X \\ Y \\ Z \\ 1 \end{bmatrix}, \quad (7)$$

where

$$P = \begin{bmatrix} 1 & 0 & 0 & 0 \\ 0 & 1 & 0 & 0 \\ 0 & 0 & 1 & 0 \\ \frac{1}{f} & 0 & 0 & 0 \end{bmatrix} \quad (8)$$

$$R = \begin{bmatrix} -\cos(\psi)\cos(\theta) & -\sin(\psi)\cos(\theta) & -\sin(\theta) & 0 \\ \cos(\psi)\sin(\theta)\sin(\phi) - \sin(\psi)\cos(\phi) & \sin(\psi)\sin(\theta)\sin(\phi) + \cos(\psi)\sin(\phi) & -\cos(\theta)\sin(\phi) & 0 \\ \cos(\psi)\sin(\theta)\cos(\phi) + \sin(\psi)\sin(\phi) & \sin(\psi)\sin(\theta)\cos(\phi) - \cos(\psi)\cos(\phi) & -\cos(\theta)\cos(\phi) & 0 \\ 0 & 0 & 0 & 1 \end{bmatrix}, \quad (9)$$

$$\text{and } T = \begin{bmatrix} 1 & 0 & 0 & -X_c \\ 0 & 1 & 0 & -Y_c \\ 0 & 0 & 1 & -Z_c \\ 0 & 0 & 0 & 1 \end{bmatrix} \quad (10)$$

are the perspective projection, rotation and translation transformation matrices, respectively, and  $f$  is the focal length. After perspective projection, we need to consider the following special cases:

- A. the region of interest degenerates to a line in the image plane because the region is too far from the camera.

B. the region of interest in the image plane becomes very large because the edge is very close to the camera.

For case A, a minimum width in the image plane is assigned in order to provide some search space for the feature detector. For case B, a maximum width in image space is defined to further restrict the region. In our experiment, for the aforementioned extreme cases, the minimum and maximum width of a region of interest are set to be 10 and 20 pixels, respectively.

### B. Defining Search Space for Horizon Line

When the vertical angular field of view is larger than  $2\theta$ , then a horizon line appears in the image (Fig. 11). The horizon is an important clue in estimating the camera orientation since it gives the roll angle information directly. Search space in the image plane is defined to locate this line.

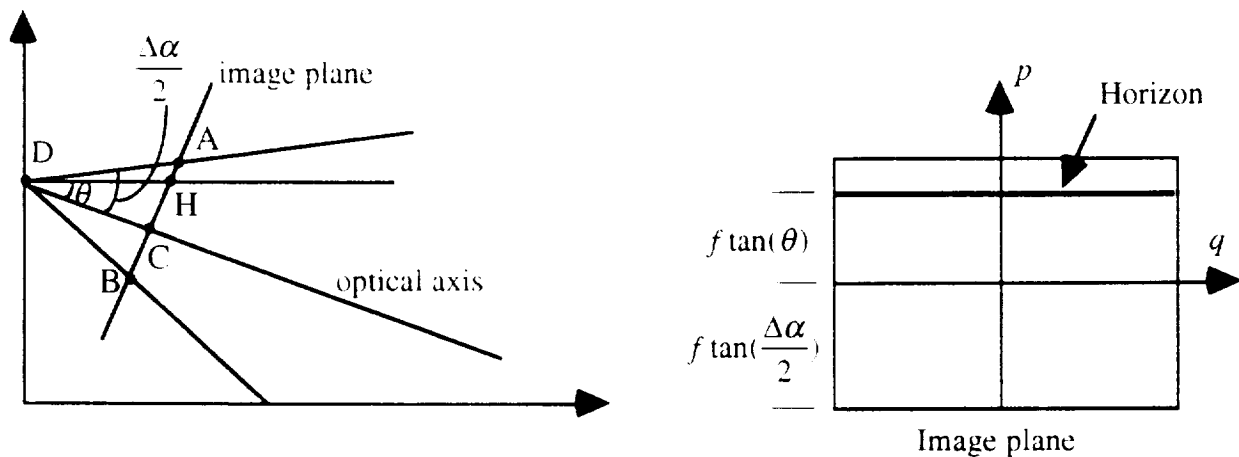


Fig. 11. Horizon line in the image.

Without loss of generality, consider the situation when the aircraft is heading towards the X axis of the world coordinate system. Assume the camera is located at point D (see Fig. 11) with pitch angle  $\theta$ , and zero yaw and roll angles. Points A and B are on the top and bottom edge of the image, respectively. The horizon will then appear horizontally in the image plane as shown. The distance between this line and the center line of the image is given by  $\overline{HC} = f \tan(\theta)$ . Since in the above analysis roll angle has been assumed to be zero, the horizon appears parallel to the horizontal axis of the image plane. For any non zero roll angle, a simple roll transformation on this line will give the horizon in the image. The associated region of interest is defined to be 10 pixels centered around the expected horizontal line in the image.

It is possible for the projection of the region of interest onto the image plane to be partially outside the image boundary. In such cases, we need to clip these regions so that the search space always remains within the confines of the image. This is done using the "polygon clip and fill" algorithm [4]. The regions of interest for both the runway and the horizon of the image sequence used in these experiment are shown in Fig.12.

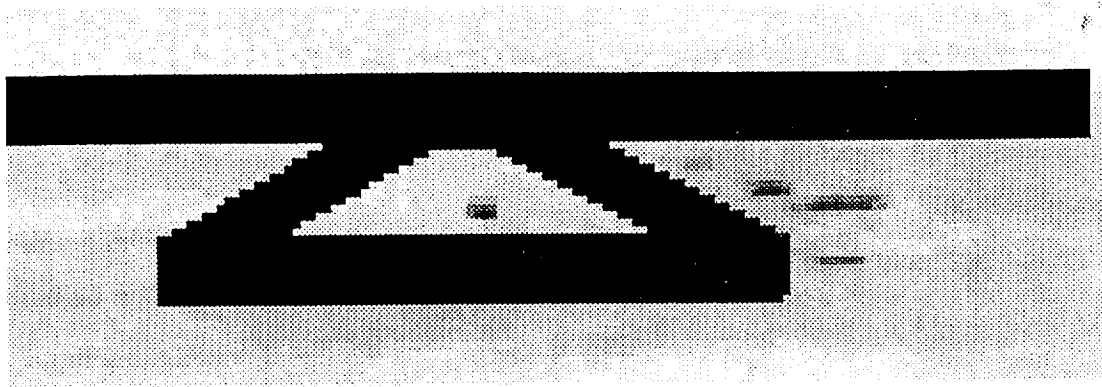


Fig. 12. Regions of interest.

## V. Runway Localization and Object Detection

### A. Runway Localization

In this part of the system we search for the expected features within the region of interest, defined by the previous module. This will significantly reduce the search time and also avoid the spurious response which is likely in such a low resolution input image. An accurate localization of the feature is necessary for estimation of motion parameters and camera pose.

A Sobel edge detector is applied to the sensor image. We then select one of the four scanning directions ( $-45^{\circ}$ ,  $0^{\circ}$ ,  $45^{\circ}$ ,  $90^{\circ}$ ) which is approximately orthogonal to the direction of the expected edge. Along each scan line we locate pixels with greatest edge strength. As the runway edge is supposed to be a straight line we fit a best line to these pixels. We also associate a measure of confidence for these detected edges based on the number of edge pixels detected along the line.

### B. Object Detection

In this section, the region inside and outside the runway/taxiways are separately checked for the existence of any stationary or moving objects. The image has three homogeneous regions, namely the sky, the runway/taxiways and the region outside the runway/taxiways. Any objects on or outside the runway/taxiways are expected to have some deviation in graylevel from their respective homogeneous background. Hence, we use histogram-based thresholding for object detection. The thresholds which determine this deviation are set to be different for different regions.

We generate a mask image which represents three homogeneous regions. Using this mask image, we generate the histogram and compute its standard deviation for each region separately (except for the sky region). The threshold value is determined as a function of the mean and the standard deviation, and any area which has graylevel lower than the threshold is considered as object regions. An object is assumed to have a reasonable size. This size restriction on the object can be used to ignore spurious responses resulting from the thresholding. Each object is then labeled based on 4-connectivity.

## VI. Experimental Results

We have tested our algorithm on a test image provided by the TRW. This image was obtained using a single pixel camera located at a fixed point in space (a camera with an array of pixels is under development). The camera was mechanically scanned to obtain a 50X150 pixel image. This is the image shown in Fig. 2. We were also provided with the model of the runway giving the 3D world coordinates of the runway corners, locations of the buildings etc. Using these data and the single image, we created a sequence of 30 frames to simulate the images from a moving camera. Frames 1 (original), 5, 10, and 15 from this sequence is shown in Fig.13(a). Edge enhanced images corresponding to these frames are shown in Fig.13(b). The regions of interest defined on these frames are shown in Fig.13(c). Delineated features superimposed on the images are shown in Fig.13(d). Although all the edges are detected accurately in this example, it is likely that one or more edges of a polygon are not detected. To handle such situations we associate a degree of importance for each edge. For example, runway edges which are closer to the camera must be detected in the image whereas those corresponding to the far end of the runway are usually very short and may or may not be detected. And overall confidence measure is associated with each detected region.

Objects detected on the runway in Frame 1 and those outside the runway are shown in Fig.14. Warning signals are generated for each object on or near runway. Algorithms to track these in successive frames and estimate camera state using motion stereo are under development.

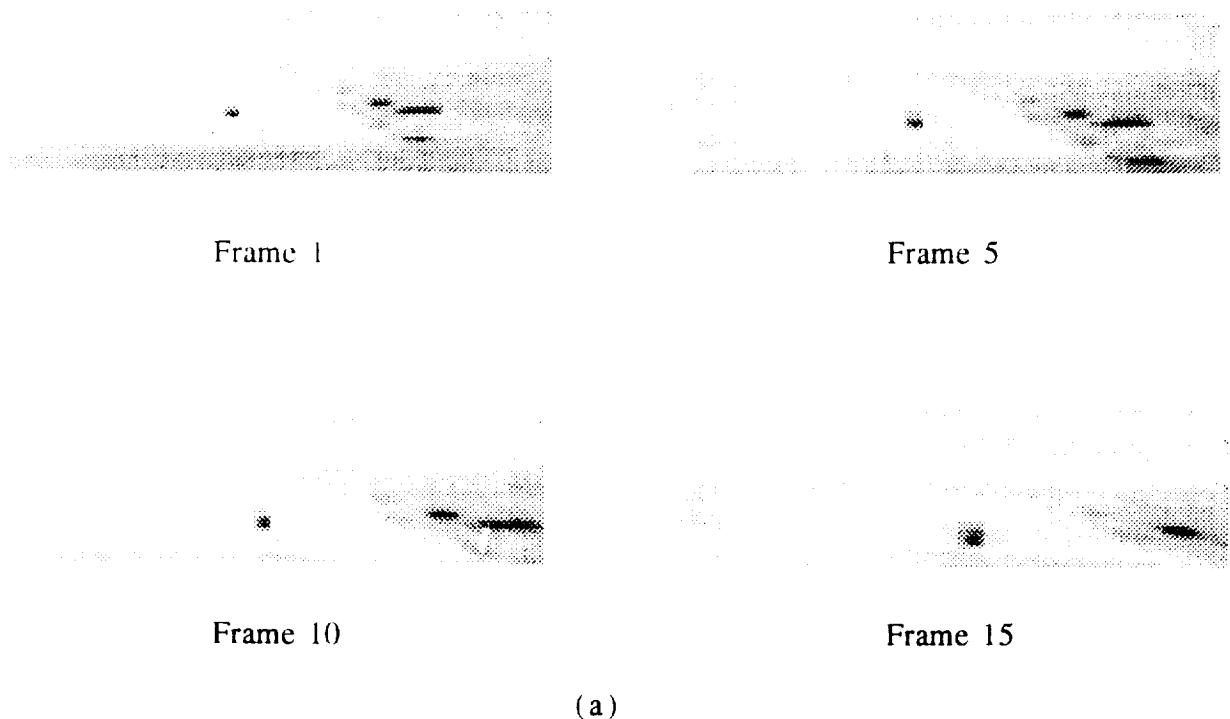
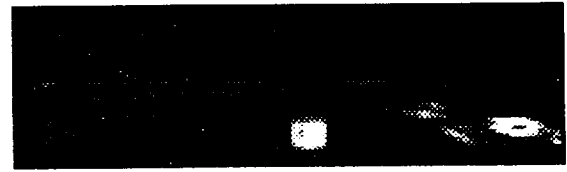
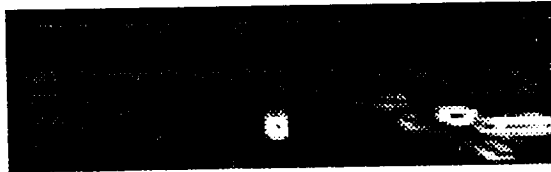
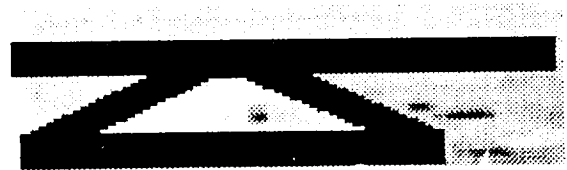
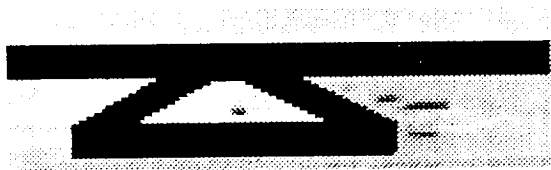


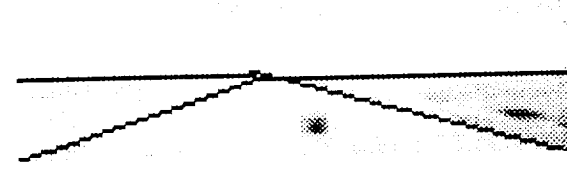
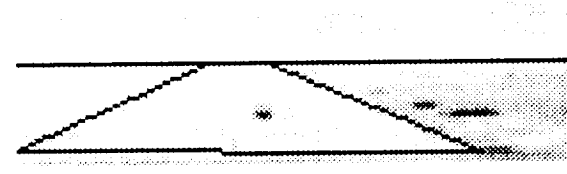
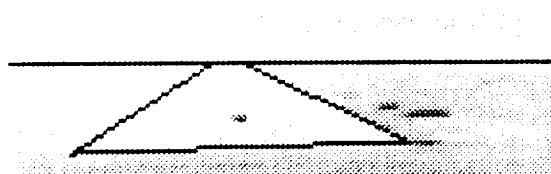
Fig. 13. The input images (a), edge images (b), regions of interest (c), and detected features superimposed on the original images (d).



(b)



(c)



(d)

Fig. 13. (continued)

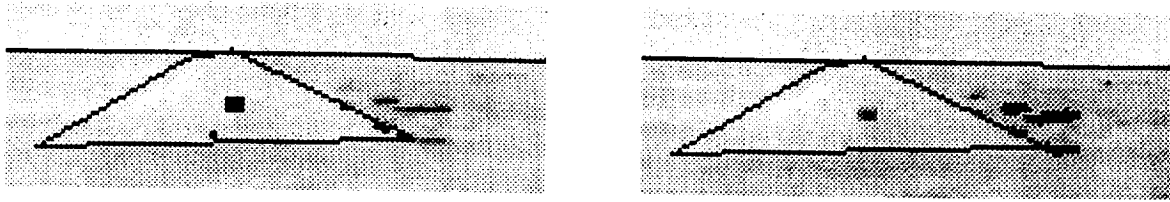


Fig. 14. Detected objects inside (left) and outside (right) the runway.

## VII. Future Work and Conclusions

In this paper, we have described a vision-based system to assist pilots during landing under restricted visibility conditions. The images obtained by a passive sensor is processed to detect major regions such as runways and objects inside and outside these regions. The image resolution is very poor; however, additional information in the form of airport geometric model, and camera position parameters are available to guide the segmentation algorithms. Objects are detected in each of these regions using thresholds computed separately for each region. Our results show that the model-based feature detection approach is quite accurate and the homogeneity assumption on regions for object detection is reasonable. The success of this model-based approach clearly depends upon the accuracy of the camera position parameters used to define search regions in the image. One of the methods for updating camera position information is triangulation using known objects. We have derived the accuracy of such an update as a function of camera characteristics and image parameters.

At this stage, our system is able to detect the runway/taxiways and the objects inside and outside the runway/taxiways in each frame and to report their positions in the image. Since we have a moving camera, moving object situation, even the stationary objects appear to be moving in the image. Work is in progress to estimate the egomotion of the camera, to distinguish moving objects from stationary ones and to estimate the velocities of the moving objects. There is also potential to obtain more accurate camera state estimation using motion stereo from image sequences compared to using GPS data alone.

## References

- [1]. Hatfield, J.J. and R.V. Parrish, "Advanced Cockpit Technology for Future Civil Transport aircraft," *Proc. 11th Annual IEEE/AESS Dayton Chapter Symposium*, Dayton Ohio, Nov. 1990.
- [2]. Young, S.K., R.A. Davidheiser, B. Hauss, P.S.C. Lee, M. Mussetto, M.M. Shoucri, and L. Yujiri, "Passive Millimeter-Wave Imaging," *TRW Space & Defense — Quest*, Vol. 13, No.2, pp. 3-20, Winter 1990/1991.
- [3]. Smith, P.N., "NASA Image Data Base User's Guide," NASA Ames Research Center, Moffett Field, CA., Version 1.0, 1990.
- [4]. Foley, J.D., A. van Dam, S.K. Feiner, and J.F. Hughes, "Computer Graphics—Principles and Practice," Addison-Wesley Publishing Co., 2nd. ed., 1990.